2022

Optical Measurements Of Liquid Film Thickness During Condensation In A Small Diameter Tube

Arianna Berto

Pascal Lavieille

Marco Azzolin

Stefano Bortolin

Marc Miscevic

See next page for additional authors

Optical measurements of liquid film thickness during condensation in a small diameter tube

Arianna BERTO[1], Pascal LAVIEILLE[2], Marco AZZOLIN[1], Stefano BORTOLIN[1], Marc MISCEVIC[2], Davide DEL COL[1]*

[1]Department of Industrial Engineering, University of Padova
Via Venezia 1, 35131 – Padova, Italy

[2]Université Toulouse III – Paul Sabatier, Laboratoire Plasma et Conversion d'Énergie - LAPLACE
118 Route de Narbonne, 31062 – Toulouse, France

* Corresponding Author: davide.delcol@unipd.it

ABSTRACT

The measurement of heat transfer coefficient together with liquid film thickness is fundamental to better understand heat transfer mechanisms involved during annular flow condensation. However, the experimental measurement of the liquid film thickness is challenging when considering small diameter channels which have recently been increasingly used by industries. The present work addresses this problem presenting experimental measurements of liquid film thickness and heat transfer coefficients during vertical downflow condensation inside a 3.38 mm inner diameter channel. The test section is composed of two heat exchangers made of copper and connected with a glass tube. Liquid film thickness measurements are performed in the glass window, while the heat transfer coefficient is measured in the two heat transfer sectors. The glass tube has been designed and machined with a special external shape that, as a lens, produces a magnification of the liquid film thickness and allows the use of a chromatic confocal sensor. The liquid film thickness is determined by coupling a shadowgraph technique with the measurements performed by the chromatic confocal sensor. These techniques allow to accurately determine the liquid film thickness without disturbing the two-phase flow. Condensation tests have been run with refrigerant R245fa at 40 °C saturation temperature and mass velocity ranging from 50 kg m^{-2} s^{-1} to 150 kg m^{-2} s^{-1}. The measured values of heat transfer coefficient and liquid film thickness are presented and analyzed together to investigate the effect of waves on the condensation heat transfer.

1. INTRODUCTION

Annular flow is the most recurrent flow regime during condensation in vertical channels. During annular flow, the heat transfer coefficient mainly depends on the liquid film thickness at the tube wall, the turbulence in the condensate film and the presence of waves at the vapor-liquid interface induced by the vapor shear stress (Gou *et al.*, 2017; Toninelli *et al.*, 2018). Accurate liquid film thickness measurements during annular flow are fundamental to evaluate the occurring heat transfer mechanisms and to develop reliable methodologies for two-phase cooling systems design. In the past decades, liquid film thickness measurements during annular flow have been mainly carried out inside large diameter channels, together with in-depth statistical analyses of the features of the interfacial waves (Azzopardi, 1986; Cioncolini & Thome, 2013). In the literature, the number of research studies dealing with liquid film thickness measurements inside minichannels during condensation of refrigerants is limited due to the technical difficulties in performing accurate measurements at such scales. A review of the experimental procedures employed for the measurement of the liquid film thickness in micro-scale is provided by Tibiriçá *et al.* (2010). Only methods based on light attenuation, liquid-vapor interface detection and light reflection were found to be suitable for measuring the liquid film thickness inside micro-channels. Moreira *et al.* (2020) performed liquid film thickness measurements in vertical upward annular flow with R245fa inside a rectangular channel (cross section 11.6 mm x 36 mm) using an optical method based on light reflection. Zhang *et al.* (2022) measured the liquid film thickness trends

of R245fa and of zeotropic mixtures of R134a/R245fa inside a 1 mm inner diameter circular channel using a CCD camera and a Laser Focus Displacement Meter (LFDM).
The combined measurement of instantaneous liquid film thickness and heat transfer coefficients enables to better understand the role of interfacial waves on the heat transfer during annular flow regime. During annular flow, the liquid-vapor interface is rippled by complex interfacial structures, which can be classified as "disturbance waves" or "ripple waves" depending on their amplitude. Extensive research has been conducted especially on high-amplitude waves, the so-called disturbance waves, which are deemed to play a key role in the heat transfer enhancement during condensation (Belt *et al.*, 2010; Vasques *et al.*, 2018). However, most of these studies are not concerned with heat transfer considerations and only few exceptions can be found in the literature (Budakli *et al.*, 2019; Zimmerman *et al.*, 2006).
In the present paper, liquid film thickness and heat transfer coefficients have been simultaneously measured during condensation in vertical downflow inside a 3.38 mm inner diameter channel. Condensation tests have been run with refrigerant R245fa at 40 °C saturation temperature. The instantaneous liquid film thickness is measured by combining the shadowgraph technique and the chromatic confocal imaging. An *ad hoc* algorithm has been developed to statistically characterize the wave structures and to better investigate how the interfacial waviness affects the heat transfer.

2. EXPERIMENTAL APPARATUS AND DATA REDUCTION

The experimental setup for condensation tests consists of a primary refrigerant loop and three auxiliary water loops. In the refrigerant circuit, a post-condenser is used to keep the refrigerant subcooled before it enters a magnetic-driven gear pump. The fluid is then vaporized and superheated in a tube-in-tube heat exchanger before entering the condensation test section. As shown in Fig. 1a), the test section is composed of two counter-current tube-in-tube heat exchangers for heat transfer measurements separated by a 40 mm long borosilicate glass tube for flow pattern visualizations and liquid film thickness measurements. The internal diameter of the test section is equal to 3.38 mm.

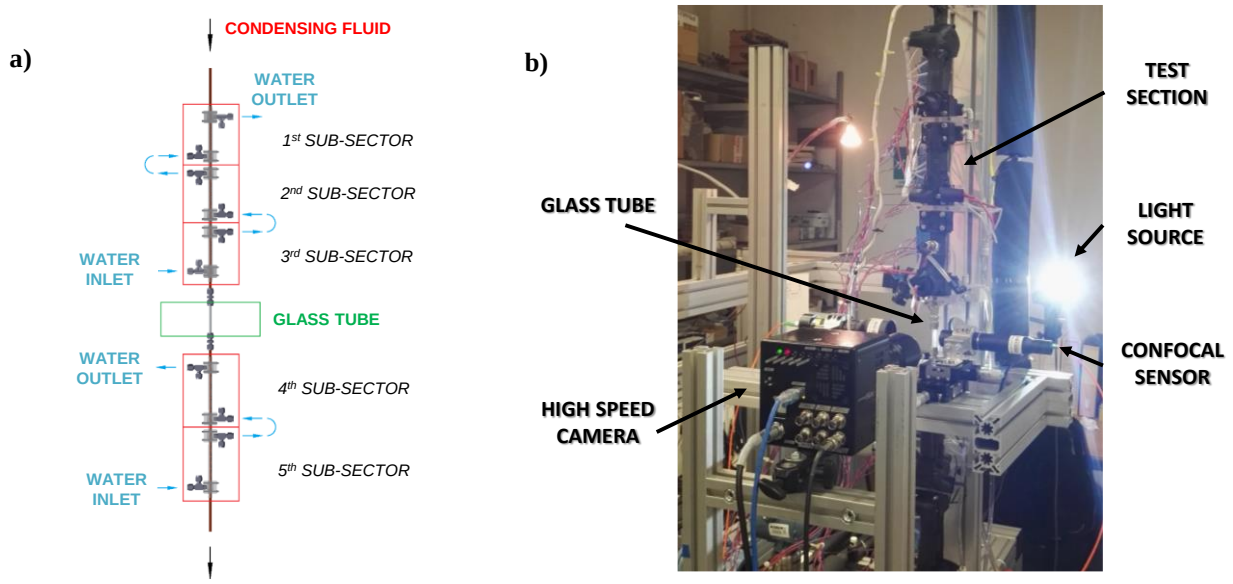

Figure 1: Experimental test rig: a) sketch of the experimental heat transfer test section; b) picture of the optical system consisting of a glass tube, a high-speed camera, a LED light source and a chromatic confocal sensor.

Each heat exchanger is divided respectively into three and two sectors: the refrigerant flows in the internal circular channel (3.38 mm inner diameter), whereas the water streams in the external annulus. A finned geometry has been machined on the external coolant side to increase the heat transfer surface and to allow the insertion of wall thermocouples. In each sector, six thermocouples are embedded in the copper wall for a total of thirty wall thermocouples installed in the test section. On the water side, two thermocouples (accuracy ±0.05 °C) and a triple-junction thermopile (accuracy ±0.03 °C) are used to check the temperature difference of the water between inlet and outlet of each sector. The refrigerant and water mass flow rates are measured by means of Coriolis mass flow meters

(accuracy of ±0.14% at 3×10^{-3} kg s^{-1} and ±0.2% at 6×10^{-4} kg s^{-1} respectively on the water and refrigerant side). The refrigerant temperatures at the inlet and outlet of the test section are measured by T-type thermocouples (accuracy ±0.05 °C), while the inlet pressure is measured using relative pressure transducers (accuracy ±5 kPa). The pressure drop along the test section is determined by two differential pressure transducers with different full scale (accuracy ±0.12 kPa at Δp > 1 kPa, accuracy ±0.1% at Δp < 1 kPa).
The experimental internal heat transfer coefficient in each *i*-th sector is calculated as follows:

$$\mathrm{HTC}_i = \frac{q_{water,i}}{A\cdot\left(T_{sat}-T_{w,mean}\right)_i} = \frac{\dot{m}_{water,i}\cdot c_{water}\cdot\Delta T_{water,i}}{A\cdot\left(T_{sat}-T_{w,mean}\right)_i} \tag{1}$$

where $q_{water,i}$ is the heat flow rate exchanged in each *i*-th sector, A is the internal heat transfer area, T_{sat} is the refrigerant saturation temperature, $T_{w,mean}$ is the wall temperature (average between the two temperatures measured in the middle of each sector), $\dot{m}_{water,i}$ is the water mass flow rate and $\Delta T_{water,i}$ is the temperature difference between inlet and outlet on the water side (measured by the *i*-th thermopile). The heat flow rate is employed to determine the enthalpy at the outlet of the *i*-th sector $h_{out,i}$ (from the measured refrigerant mass flow rate and the inlet enthalpy) and thus the outlet vapour quality $x_{out,i}$, using the following equations:

$$h_{out,i} = h_{in,i} - \frac{q_{water,i}}{\dot{m}_{ref}} \tag{2}$$

$$x_{out,i} = \frac{h_{out,i}-h_L}{h_V-h_L} \tag{3}$$

The mean vapor quality in each *i*-th sector is calculated as the average between the inlet and outlet values. The vapor quality change in each sector is kept lower than 0.2 during the experimental tests, thus the experimental heat transfer coefficient can be assumed as a quasi-local value. The thermodynamic properties of the tested fluid are computed using REFPROP 9.1 (Lemmon *et al.*, 2018). Considering the present experimental database, the mean expanded uncertainty of the heat transfer coefficient (coverage factor equal to 2) is about ±3%, while the maximum uncertainty on the vapor quality is equal to ±0.01 at G = 50 kg m^{-2} s^{-1}. Additional information on the experimental setup and the data reduction procedure is reported in Azzolin *et al.* (2019).
The optical system for liquid film thickness measurements and flow pattern visualizations consists of a borosilicate glass tube, a LED light source, a high-speed camera and a chromatic confocal sensor. Flow pattern visualizations have been recorded simultaneously with heat transfer coefficient and liquid film thickness measurements using Photron® FASTCAM Mini UX100 high-speed camera, coupled with Navitar® Zoom 7000 18-108 mm macro lens and a LED illumination system. The acquisition frame rate is fixed at 1000 fps. The external side of the glass tube, consisting of two symmetric curved parts and two parallel flat sides, has been designed and machined to measure the liquid film thickness with the confocal sensor and, at the same time, magnify the liquid film for the shadowgraph technique. The liquid film thickness is deduced from calibration curves obtained by coupling the shadowgraph technique, through which the vapor-liquid interface can be detected from the images recorded by the high-speed camera using a ray tracing model, and the confocal chromatic sensor, which allows punctual liquid film thickness measurements up to 300 μm (provided that the slope of the interface is lower than 28°). A picture of the optical system for liquid film thickness measurements and flow pattern visualizations is reported in Fig. 1b). The uncertainty on the film thickness is about ±2 μm in the case of the confocal sensor measurements, while it ranges between ±10 μm and ±15 μm when using the shadowgraph technique. Additional information about the present technique is reported in Berto *et al.* (2021).

3. EXPERIMENTAL RESULTS

The experimental results reported in this Section have been obtained with R245fa during condensation in vertical downflow at 40 °C saturation temperature and mass velocity from 50 to 150 kg m^{-2} s^{-1}. The experimental heat transfer coefficients are reported versus vapor quality in Fig. 2. The heat transfer coefficient is found to increase with mass velocity and vapor quality. In particular, at mass velocity G > 75 kg m^{-2} s^{-1}, the effect of the mass velocity on the condensation heat transfer is more pronounced: indeed, while at G = 75 kg m^{-2} s^{-1} the heat transfer coefficient

is on average 10% higher than that at G = 50 kg m^{-2} s^{-1}, the heat transfer increase at G = 100 kg m^{-2} s^{-1} ranges from 30% to 40% with respect to G = 75 kg m^{-2} s^{-1} considering the whole vapor quality range.

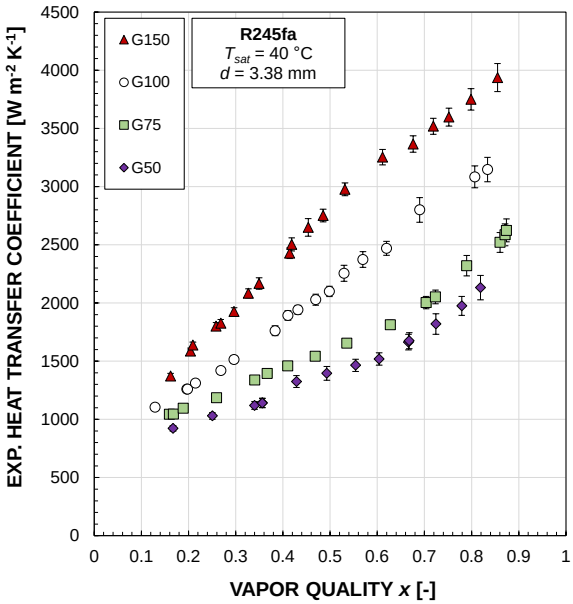

Figure 2: Condensation heat transfer coefficients measured with refrigerant R245fa inside the 3.38 mm inner diameter tube (vertical downflow) at 40 °C saturation temperature and mass velocity G from 50 kg m^{-2} s^{-1} to 150 kg m^{-2} s^{-1}

Fig. 3 shows the flow pattern visualizations performed at mass velocity equal to 50, 75, 100 and 150 kg m^{-2} s^{-1} and different vapor qualities. As shown in Fig. 3, annular wavy flow is detected for all the operating conditions. The interface, depending on vapor quality and mass velocity, is rippled by waves of different amplitude and frequency. In Fig. 3, at G = 50 kg m^{-2} s^{-1} and low vapor quality (x < 0.4), the vapor-liquid interface displays small-amplitude waves, which are found to increase in frequency at high vapor quality (x > 0.7). At G = 75 kg m^{-2} s^{-1} and G = 100 kg m^{-2} s^{-1}, the vapor-liquid interface is disturbed by occasional high-amplitude disturbance waves at low vapor quality and the waviness is generally more pronounced with respect to G = 50 kg m^{-2} s^{-1}. With the increasing vapor quality and mass velocity, the condensate interface is characterized by high-frequency and low-amplitude waves due to the greater vapor shear stress acting on the condensate film.

In order to analyze the liquid film thickness measurements and correlate them with the heat transfer results, an *ad hoc* algorithm has been developed in Matlab® for the statistical characterization of the interfacial structures. The mean liquid film thickness and the base liquid film thickness are calculated for all the operating conditions as suggested by Vasques *et al.* (2018). The mean liquid film thickness δ_{mean} is defined as the arithmetic mean of N = 3100 instantaneous values δ_i recorded during the acquisition time (3.1 seconds):

$$\delta_{mean} = \frac{1}{N}\sum_{i=1}^{N}\delta_i \tag{4}$$

The base liquid film thickness δ_{base}, which is related to the liquid substrate between subsequent high-amplitude waves, is obtained by firstly identifying the local minima and maxima in the temporal film thickness records, and then selecting only the M points whose values are below the mean film thickness:

$$\delta_{base} = \frac{1}{M}\sum_{j=1}^{M}\delta_j \qquad \delta_j \le \delta_{mean} \tag{5}$$

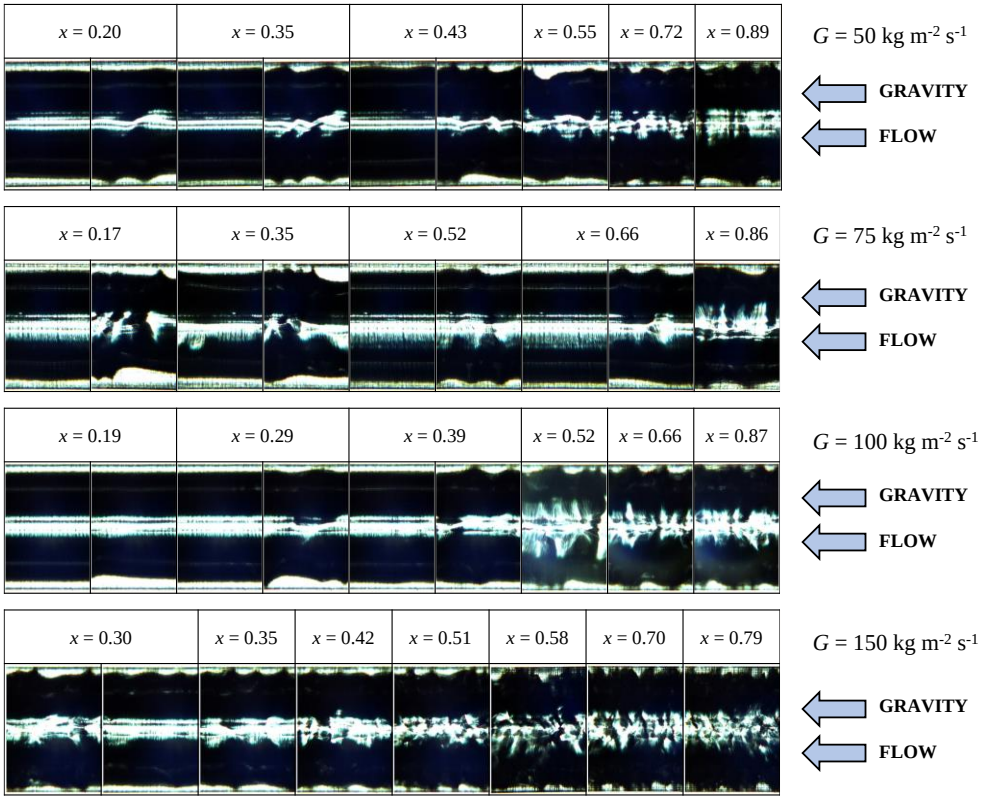

Figure 3: Flow pattern visualizations at different vapor quality during R245fa downflow condensation inside the 3.38 mm inner diameter tube and 40 °C saturation temperature. Mass velocity G ranges between 50 kg m^{-2} s^{-1} and 150 kg m^{-2} s^{-1}

In the literature, the mean liquid film thickness is typically deemed to be representative of the temporal liquid film thickness evolution; however, it may not provide sufficient information when several disturbance waves are present. Instead, the base liquid film thickness does not account for the presence of high- and medium-amplitude waves at the interface and may be useful to understand the role of the liquid substrate in the heat transfer mechanisms if correlated to heat transfer coefficient data.
Moreover, to evaluate the average deviation of the instantaneous liquid film thickness data from δ_{mean} in the whole acquisition time (3.1 s), the R_a parameter can be defined as follows:

$$R_a = \frac{1}{N}\sum_{i=1}^{N}\left|\left(\delta_i - \delta_{mean}\right)\right| \tag{6}$$

The calculated mean and base film thickness values, together with R_a parameter, are reported in Table 1 for R245fa at mass velocity equal to 50, 75, 100 and 150 kg m^{-2} s^{-1} and in the vapor quality ranges x = 0.27-0.29 and x = 0.56-0.59. From Table 1, it can be observed that both the mean and the base liquid film thickness values decrease with the increasing mass velocity and vapor quality. In the vapor quality range x = 0.27-0.29, δ_{mean} is reduced by 5.55% when the mass velocity is increased from 50 kg m^{-2} s^{-1} to 75 kg m^{-2} s^{-1}, by 6.4% from 75 kg m^{-2} s^{-1} to 100 kg m^{-2} s^{-1} and by 20.5% from 100 kg m^{-2} s^{-1} to 150 kg m^{-2} s^{-1}. The same applies to the base liquid film thickness values δ_{base}, which are decreased by 20.2% from 50 kg m^{-2} s^{-1} to 75 kg m^{-2} s^{-1}, by 12.9% from 75 kg m^{-2} s^{-1} to 100 kg m^{-2} s^{-1} and by 20.9% from 100 kg m^{-2} s^{-1} to 150 kg m^{-2} s^{-1}. At x = 0.56-0.59 the mean/base liquid film thickness reduction with mass velocity is more evident with respect to x = 0.27-0.29 when the mass velocity is increased from 50 kg m^{-2} s^{-1} to 75 kg m^{-2} s^{-1} (-22.2% for δ_{mean}, - 33.4% for δ_{base}), while at higher G values it is less significant (from 75 kg m^{-2} s^{-1} to 100 kg m^{-2} s^{-1}: -16.2% for δ_{mean}, - 6.8% for δ_{base}).

At x = 0.27-0.29 and G = 75 kg m^{-2} s^{-1} the R_a parameter values are doubled compared to G = 50 kg m^{-2} s^{-1} and this is due to the appearance of disturbance waves induced by the vapor shear stress acting on the liquid-vapor interface. This also helps explain the marked decrease of the base liquid film thickness observed from 50 to 75 kg m^{-2} s^{-1}, as the high-amplitude disturbance waves carry significant portions of the condensate and promote the thinning of the base film thickness. A slight increase in the R_a values is detected from G = 75 kg m^{-2} s^{-1} to G = 100 kg m^{-2} s^{-1} (+1.7%), while at G = 150 kg m^{-2} s^{-1} R_a parameter decreases due to the higher vapor shear stress acting on the liquid-vapor interface and thus reduced mean liquid film thickness. At x = 0.56-0.59, the R_a parameter value still displays the highest value at G = 75 kg m^{-2} s^{-1} and decreases with the increasing G value. The analysis of the average film thickness data highlights that a sudden change in the film thickness features occurs starting from 50-75 kg m^{-2} s^{-1}.

Table 1. Parameters used to characterize the liquid film thickness of R245fa at mass velocity G equal to 50, 75, 100 and 150 kg m^{-2} s^{-1} (vapor quality x = 0.27-0.29 and x = 0.56-0.59)

Vapor quality x [-]	x = 0.27-0.29				x = 0.56-0.59		
Mass velocity G [kg m^{-2} s^{-1}]	G50	G75	G100	G150	G50	G75	G100
δ_{mean} [μm]	144.33	136.32	127.62	101.48	101.18	78.71	65.93
δ_{base} [μm]	99.89	79.69	69.38	54.91	59.99	39.98	37.27
R_a [μm]	33.30	66.79	67.91	52.68	30.93	33.50	26.15

To complete the characterization of the interfacial features, the power spectral density (PSD) in the frequency domain of the liquid film thickness records of R245fa has been calculated. The PSDs are obtained by averaging the results of the Welch algorithm, using a Hamming window with 50% overlap between three equal segments of a specific liquid film thickness time series. The peak in the power spectral density of a temporal film thickness profile identifies the dominant frequency of the high-amplitude disturbance waves. Fig. 4 shows the PSDs of wave frequency of R245fa at mass velocity equal to 50, 75 and 100 kg m^{-2} s^{-1} and in the vapor quality range x = 0.27-0.29. At G = 50 kg m^{-2} s^{-1} the PSD covers frequencies up to 100 Hz and displays a peak at 9 Hz. At G = 75 kg m^{-2} s^{-1} the main frequency peak is still at 9 Hz, but the PSD value is much higher than the one observed at G = 50 kg m^{-2} s^{-1} due to the formation of disturbance waves which display high amplitude (δ_{max} = 1100 μm at G = 75 kg m^{-2} s^{-1}, δ_{max} = 367 μm at G = 50 kg m^{-2} s^{-1}). Such disturbance waves are also responsible for the base liquid film thickness reduction observed from G = 50 kg m^{-2} s^{-1} to G = 75 kg m^{-2} s^{-1} (Table 1). Moreover, at G = 75 kg m^{-2} s^{-1} the range of detected frequencies is wider compared to G = 50 kg m^{-2} s^{-1}. At G = 100 kg m^{-2} s^{-1} the PSD curve is more flattened with respect to smaller G values due to the coexistence of both large-scale interfacial structures, with dominant frequency of 16 Hz and 55 Hz, and small-amplitude ripples, which display higher frequency.

In Fig. 5 the PSDs of wave frequency of R245fa in the vapor quality range x = 0.56-0.59 are reported at mass velocity equal to 50, 75 and 100 kg m^{-2} s^{-1}. The PSD values corresponding to the frequency peak at G = 50 kg m^{-2} s^{-1} and G = 75 kg m^{-2} s^{-1} are comparable, but the peak is shifted towards slightly higher frequency for G = 75 kg m^{-2} s^{-1}. Furthermore, the PSD curve at G = 50 kg m^{-2} s^{-1} varies within a narrow range (10-150 Hz), whereas at 75 kg m^{-2} s^{-1} and 100 kg m^{-2} s^{-1} the combination of ripple waves, showing periodical features, and residual medium-amplitude waves causes a broader spectrum of frequencies (up to 300-400 Hz). At G = 100 kg m^{-2} s^{-1} the PSD values are smaller compared to lower mass velocities due to the reduction in the liquid film thickness height with the increasing G value (i.e. increasing vapor shear stress effect on the interface).

During annular condensation with laminar liquid film and no waves (no turbulence and recirculation effects are present), the heat transfer coefficient (HTC_{lam}) is inversely proportional to the conductive thermal resistance across the condensate and thus to the liquid film thickness, as indicated by Eq. (7):

$$HTC_{lam} = \frac{\lambda_L}{\delta} \tag{7}$$

where λ_L is the thermal conductivity of the liquid and δ is the mean or base liquid film thickness.

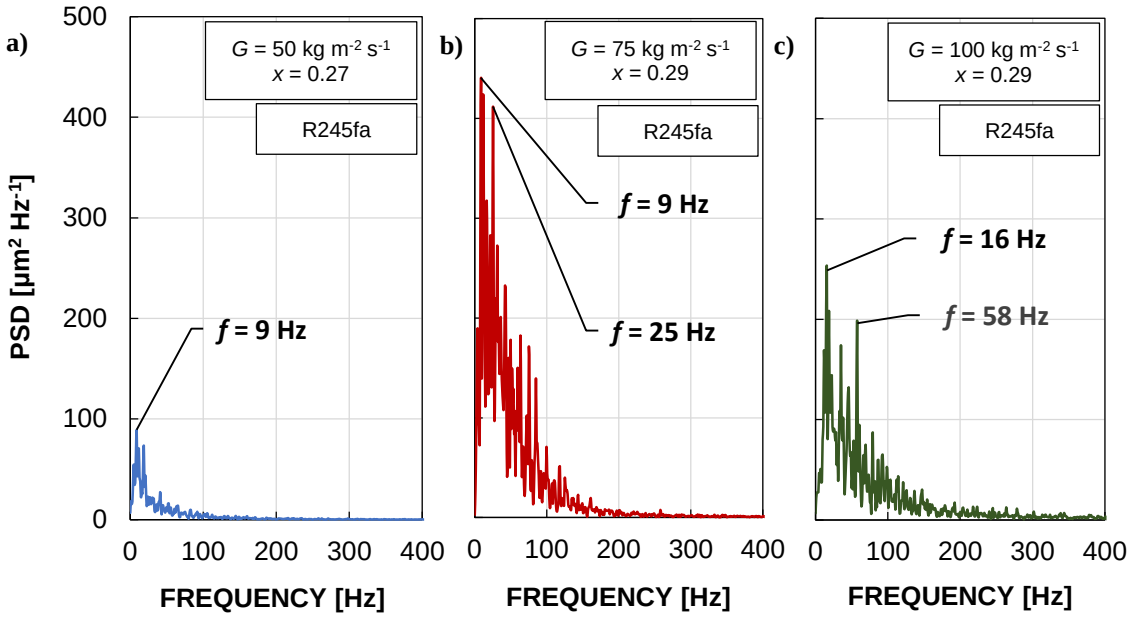

Figure 4: Power spectral density (PSD) of wave frequency for R245fa, obtained using the Welch method, at 40 °C saturation temperature, mass velocity equal to 50, 75 and 100 kg m^{-2} s^{-1} and vapor quality x = 0.27-0.29

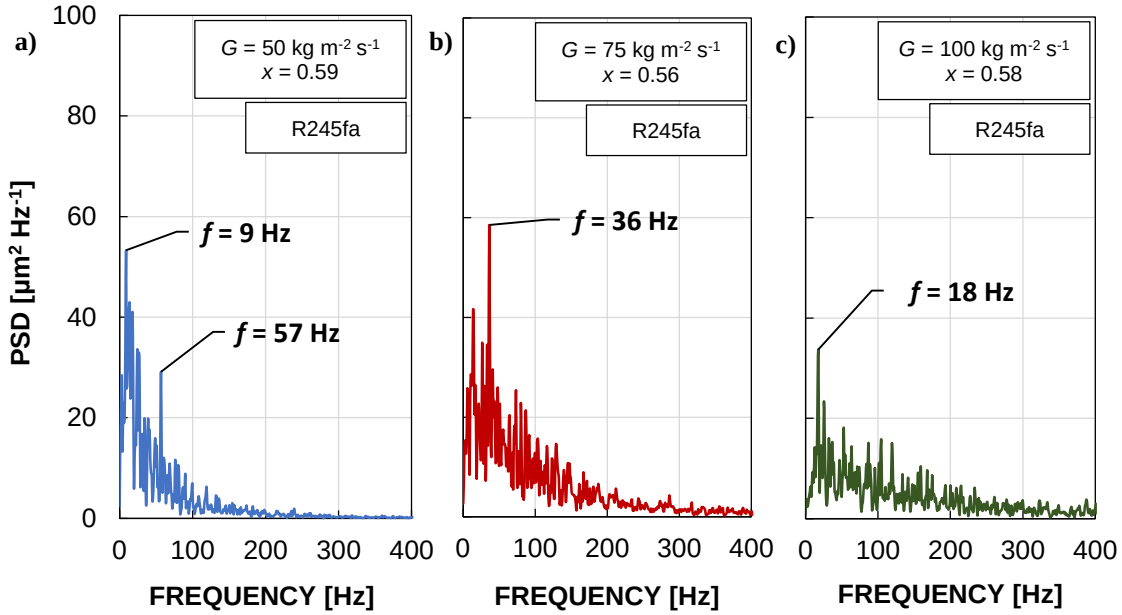

Figure 5: Power spectral density (PSD) of wave frequency for R245fa, obtained using the Welch method, at 40 °C saturation temperature, mass velocity equal to 50, 75 and 100 kg m^{-2} s^{-1} and vapor quality x = 0.56-0.59

According to Eq. (7), the heat transfer coefficient variation at a specific mass velocity with respect to a reference G value can be related to the mean/base liquid film thickness ratio as indicated in the following equation:

$$\frac{\mathrm{HTC}_G}{\mathrm{HTC}_{G,reference}} \propto \frac{\delta_{G,reference}}{\delta_G} \tag{8}$$

In the present analysis, the heat transfer coefficient measured at G = 50 kg m^{-2} s^{-1} (HTC$_{G50}$) and the liquid film thickness measured at the same mass velocity (δ_{G50}) have been taken as the reference case. In Fig. 6, histograms show the variation of the ratios of mean liquid film thickness, base liquid film thickness and heat transfer coefficient with mass velocity and vapor quality. From Fig. 6a) it can be observed that, at x = 0.30, the heat transfer coefficient variation is more related to the thickness of the base liquid film rather than the overall liquid film thickness. In particular, at G = 100 kg m^{-2} s^{-1} and G = 150 kg m^{-2} s^{-1} the heat transfer coefficient ratio is higher than the base liquid film thickness ratio, whereas the mean liquid film thickness ratio is much lower. Therefore, at such conditions, the main thermal resistance is concentrated inside the base liquid film, below the wavy region. As shown in Fig. 4a), starting from G = 75 kg m^{-2} s^{-1}, high-amplitude disturbance waves are found to appear and the turbulence zones within the wave crests or in the liquid film may contribute to the heat transfer enhancement (Zadrazil & Markides, 2014). Instead, at x = 0.60 (Fig. 6b), the heat transfer coefficient variation is comparable to both the mean and the base film thickness values. At this condition, as the amplitude of the waves reduces while their frequency increases, the mean and the base film thickness values are similar. In general, at high vapor quality the thermal conduction through the liquid film represents the main contribution and the heat transfer coefficient increase is mainly due to the thinning of the liquid film.

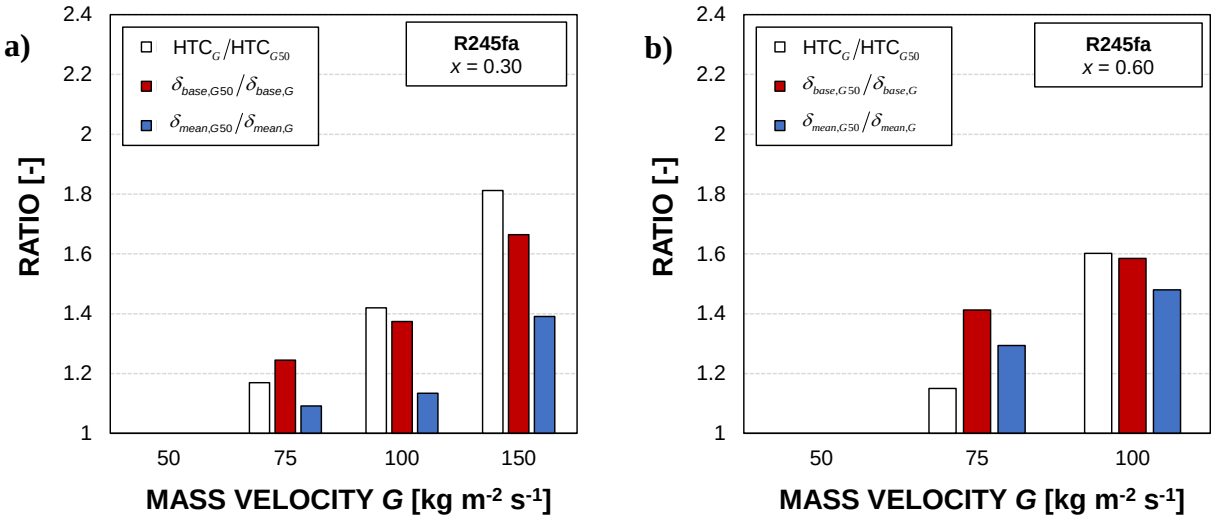

Figure 6: Comparison among variation of heat transfer coefficient, mean liquid film thickness and base liquid film thickness of R245fa with respect to the reference condition at G = 50 kg m^{-2} s^{-1}: a) vapor quality x = 0.30; b) vapor quality x = 0.60

4. CONCLUSIONS

Condensation tests in vertical downflow have been carried out inside a 3.38 mm inner diameter tube with refrigerant R245fa. The condensation process has been studied by simultaneously measuring the heat transfer coefficient and the liquid film thickness, which is evaluated by combining the shadowgraph technique and the chromatic confocal imaging. The flow pattern visualizations show that the flow is always annular with waves of different amplitudes depending on the operating conditions. The analysis of the power spectral density in the frequency domain of the liquid film thickness temporal records highlights the occurrence of high-amplitude disturbance waves at mass velocity G = 75-100 kg m^{-2} s^{-1} and low vapor quality (x = 0.3). An *ad hoc* algorithm has been developed in Matlab® for the statistical characterization of the interfacial structures. The mean liquid film thickness and the base liquid film thickness resulting from the algorithm are correlated to the experimental heat transfer coefficients of R245fa in order to assess the relative contribution of film thinning and interfacial waviness on the heat transfer. At G > 75 kg m^{-2} s^{-1} and low vapour quality, the thinning of the liquid film and the turbulence effects associated to the disturbance waves contribute to the heat transfer enhancement. Instead, at high vapour quality, the heat transfer enhancement with increasing mass velocity is mainly related to the thinning of the liquid film.

NOMENCLATURE

A	heat transfer area	(m^2)
c	specific heat	($J\ kg^{-1}\ K^{-1}$)
f	wave frequency	(Hz)
G	mass velocity	($kg\ m^{-2}\ s^{-1}$)
h	specific enthalpy	($J\ kg^{-1}$)
HTC	heat transfer coefficient	($W\ m^{-2}\ K^{-1}$)
$\dot{m}$	mass flow rate	($kg\ s^{-1}$)
q	heat flow rate	(W)
R_a	average deviation of the instantaneous liquid film thickness data from δ_{mean}	(μm)
T	temperature	(°C)
x	vapor quality	(-)

Greek symbols

Δp	pressure drop	(kPa)
ΔT	temperature difference	(°C)
λ	thermal conductivity	($W\ m^{-1}\ K^{-1}$)
δ	liquid film thickness	(μm)

Subscript

base	base
G	mass velocity
i	*i*-th element
in	inlet
L	liquid
lam	laminar
mean	mean
out	outlet
ref	refrigerant
sat	saturation
V	vapor
wall	wall

REFERENCES

Azzolin, M., Bortolin, S., & Del Col, D. (2019). Convective condensation at low mass flux: Effect of turbulence and tube orientation on the heat transfer. *International Journal of Heat and Mass Transfer*, *144*, 118646. https://doi.org/10.1016/j.ijheatmasstransfer.2019.118646

Azzopardi, B. J. (1986). Disturbance wave frequencies, velocities and spacing in vertical annular two-phase flow. *Nuclear Engineering and Design*, *92*, 121–133.

Belt, R. J., Van't Westende, J. M. C., Prasser, H. M., & Portela, L. M. (2010). Time and spatially resolved measurements of interfacial waves in vertical annular flow. *International Journal of Multiphase Flow*, *36*, 570–587. https://doi.org/10.1016/j.ijmultiphaseflow.2010.03.004

Berto, A., Lavieille, P., Azzolin, M., Bortolin, S., Miscevic, M., & Del Col, D. (2021). Liquid film thickness and heat transfer measurements during downflow condensation inside a small diameter tube. *International Journal of Multiphase Flow*, *140*, 103649. https://doi.org/10.1016/j.ijmultiphaseflow.2021.103649

Budakli, M., Gambaryan-Roisman, T., & Stephan, P. (2019). Gas-driven thin liquid films: Effect of interfacial shear on the film waviness and convective heat transfer. *International Journal of Thermal Sciences*, *146*, 106077. https://doi.org/10.1016/j.ijthermalsci.2019.106077

Cioncolini, A., & Thome, J. R. (2013). Liquid film circumferential asymmetry prediction in horizontal annular two-phase flow. *International Journal of Multiphase Flow*, *51*, 44–54. https://doi.org/10.1016/j.ijmultiphaseflow.2012.12.003

Gou, J., Wang, B., & Shan, J. (2017). Development of an analytical model for pure vapor downflow condensation in a vertical tube. *Nuclear Engineering and Design*, *320*, 346–360.

https://doi.org/10.1016/j.nucengdes.2017.05.032
Lemmon, E. W., Bell, I. H., Huber, M. L., & McLinden, M. O. (2018). *NIST Standard Reference Database 23: Reference Fluid Thermodynamic and Transport Properties (REFPROP), Version 9.1*.
Moreira, T. A., Morse, R. W., Dressler, K. M., Ribatski, G., & Berson, A. (2020). Liquid-film thickness and disturbance-wave characterization in a vertical, upward, two-phase annular flow of saturated R245fa inside a rectangular channel. *International Journal of Multiphase Flow*. https://doi.org/10.1016/j.ijmultiphaseflow.2020.103412
Tibiriçá, C. B., do Nascimento, F. J., & Ribatski, G. (2010). Film thickness measurement techniques applied to micro-scale two-phase flow systems. *Experimental Thermal and Fluid Science*, *34*, 463–473. https://doi.org/10.1016/j.expthermflusci.2009.03.009
Toninelli, P., Bortolin, S., Azzolin, M., & Col, D. Del. (2018). Visualization and Numerical Simulations of Condensing Flow in Small Diameter Channels. *Heat Transfer Engineering*. https://doi.org/10.1080/01457632.2018.1443255
Vasques, J., Cherdantsev, A., Cherdantsev, M., Isaenkov, S., & Hann, D. (2018). Comparison of disturbance wave parameters with flow orientation in vertical annular gas-liquid flows in a small pipe. *Experimental Thermal and Fluid Science*, *97*, 484–501. https://doi.org/10.1016/j.expthermflusci.2018.03.020
Zadrazil, I., & Markides, C. N. (2014). An experimental characterization of liquid films in downwards co-current gas-liquid annular flow by particle image and tracking velocimetry. *International Journal of Multiphase Flow*, *67*(S), 42–53. https://doi.org/10.1016/j.ijmultiphaseflow.2014.08.007
Zhang, Y., Jia, L., Dang, C., & Qi, Z. (2022). Measurements of the liquid film thickness for annular flow during flow condensation in a circular tube. *International Journal of Heat and Mass Transfer*, *187*, 122552. https://doi.org/10.1016/j.ijheatmasstransfer.2022.122552
Zimmerman, R., Gurevich, M., Mosyak, A., Rozenblit, R., & Hetsroni, G. (2006). Heat transfer to air-water annular flow in a horizontal pipe. *International Journal of Multiphase Flow*, *32*, 1–19. https://doi.org/10.1016/j.ijmultiphaseflow.2005.09.001

ACKNOWLEDGEMENTS

The authors acknowledge the financial support of the European Space Agency (ESA) through the MAP Condensation program. AERMEC SpA is acknowledged for funding a researcher position.